Supporting Information

In situ photo-derived MnOOH collaborating with Mn$_2$Co$_2$C@C dual cocatalysts boost photocatalytic overall water splitting

Xunfu zhou,[a] Jinmei Li,[a] Xin Cai,[a] Qiongzhi Gao,[a] Shengsen Zhang,[a] Siyuan Yang,*[a] Hongqiang Wang,[a] Xinhua Zhong [ab] and Yueping Fang*[abc]

[a] Key Laboratory for Biobased Materials and Energy of Ministry of Education, College of Materials and Energy, South China Agricultural University, 483 Wushan Road, Guangzhou 510642, China.
[b] Guangdong Laboratory for Lingnan Modern Agriculture, Guangzhou, 510642, China.
[c] Guangxi Key Laboratory of Low Carbon Energy Materials, School of Chemistry & Pharmaceutical Sciences, Guangxi Normal University, Guilin 541004, China.
* Corresponding author E-mail address: ypfang@scau.edu.cn (Yueping Fang); siyuan_yang@scau.edu.cn (Siyuan Yang);

Contents

Part I: Experimental Section

Part II: Supplementary Results

Part III: References

Part I: Experimental Section

Chemical reagents

Potassium hexacyanocobaltate ($K_3[Co(CN)_6]$), sodium citrate tribasic dihydrate ($C_6H_5Na_3O_7 \cdot 2H_2O$), manganese acetate ($Mn(CH_3COO)_2 \cdot 4H_2O$), strontium carbonate ($SrCO_3$), chloroplatinic acid hexahydrate ($H_2PtCl_6 \cdot 6H_2O$), cobalt nitrate hexahydrate ($Co(NO_3)_2 \cdot 6H_2O$) and manganese nitrate tetrahydrate ($Mn(NO_3)_2 \cdot 4H_2O$) were sourced from Aladdin. TiO_2 (P25) was purchased from Degussa. Urea was bought from Damao Chemical Reagent Factory. All the involved chemical reagents were used as purchased and not further purified.

Materials preparation

Preparation of $Mn_3[Co(CN)_6]_2 \cdot xH_2O$ and $Mn_2Co_2C@C/Mn_2N_{0.86}$. Typically, $Mn(CH_3COO)_2 \cdot 4H_2O$ (6.5 mmol) and $C_6H_5Na_3O_7 \cdot 2H_2O$ (6.5 mmol) were dissolved in 400 mL deionized water. $K_3Co(CN)_6$ (6.0 mmol) was then added to the above solution. The solution was vigorous stirred for 48 hours. The precipitate of Prussian blue analogue (denoted as PBA-CoMn) was separated by centrifugation, and dried at 80°C overnight. The $Mn_2Co_2C@C/Mn_2N_{0.86}$ (denoted as MCMN for simplicity) nanocomposites were obtained by the pyrolysis of PBA-CoMn at 600°C for 4 hours in N_2 flow.

Preparation of $Mn_2Co_2C@C$. Typically, $Co(NO_3)_2 \cdot 6H_2O$ (1.0 mmol) and $Mn(NO_3)_2 \cdot 4H_2O$ (5.0 mmol) were dissolved in 100 mL deionized water, named as solution A. $K_3Co(CN)_6$ (4.0 mmol) was dissolved in 100 mL deionized water, named as solution B. Solution B was then added to solution A under vigorous stirring. The mixed solution was agitated for 5 min then aged for 24 hours. The precipitate was separated

2

by centrifugation, and dried at 80°C overnight. The $Mn_2Co_2C@C$ nanoparticles were obtained by the pyrolysis of PBA-CoMn at 800°C for 2 hours in N_2 flow.

Preparation of hollow carbon spheres. The $Mn_2Co_2C@C$ nanoparticles were dispersed in HCl solution (1.0 M) and then stirred for 8 hours. After centrifuged and dried, the hollow carbon spheres (denoted as HCS) were obtained.

Preparation of g-C_3N_4. 50 g of urea was placed in a porcelain crucible and heated at 550°C for 2 hours (ramping rate 5°C min^{-1}) in static air. Finally, g-C_3N_4 powder was obtained after cooling to room temperature.

Preparation of $Mn_2Co_2C@C/Mn_2N_{0.86}$/g-C_3N_4, g-C_3N_4/$Mn_2Co_2C@C$ and g-C_3N_4/hollow carbon spheres. 0.3 g of g-C_3N_4 powder and different weight percentages of $Mn_2Co_2C@C/Mn_2N_{0.86}$ powder (15, 20, 25, 30 and 35 wt %) were together dispersed in 1.0 mL of ethanol, and ground in an agate mortar until the volatilization of ethanol. Then another 1.0 mL of ethanol was added, and the mixture was ground until the volatilization of ethanol again. After the mechanically grinding procedure, the $Mn_2Co_2C@C/Mn_2N_{0.86}$ nanocomposites were uniformly loaded on the surface of g-C_3N_4 with a firm contact. Finally, the products were obtained after dried at 80°C for 4 hours, and denoted as MCMN/CN-15, MCMN/CN-20, MCMN/CN-25, MCMN/CN-30 and MCMN/CN-35, respectively. The g-C_3N_4/$Mn_2Co_2C@C$ (15 wt % percentage of $Mn_2Co_2C@C$) and g-C_3N_4/hollow carbon spheres (15 wt % percentage of hollow carbon spheres) photocatalysts were obtained by using the identical method, and denoted as CN/MC-15 and CN/HCS-15, respectively.

Preparation of g-C$_3$N$_4$-Pt. 0.2 g of g-C$_3$N$_4$ powder was dispersed in 85.0 mL water and 15.0 mL triethanolamine, then the calculated H$_2$PtCl$_6$ solution was added. The mixed solution was evacuated and irradiated by UV-vis light for 2 hours. Finally, the mixed suspension was filtered, washed and dried, the g-C$_3$N$_4$-Pt (1 wt %) was obtained as a reference.

Preparation of Mn$_2$Co$_2$C@C/Mn$_2$N$_{0.86}$/SrTiO$_3$. Firstly, SrCO$_3$ (50 mmol) and TiO$_2$ (P25, 50 mmol) were mixed evenly, then heated at 1150°C for 10 hours (ramping rate 5°C min^{-1}) in static air. Finally, SrTiO$_3$ powder was obtained after cooling to room temperature. Mn$_2$Co$_2$C@C/Mn$_2$N$_{0.86}$/SrTiO$_3$ samples were obtained by using the same way of preparing the Mn$_2$Co$_2$C@C/Mn$_2$N$_{0.86}$/g-C$_3$N$_4$ samples. Samples with Mn$_2$Co$_2$C@C/Mn$_2$N$_{0.86}$ percentages of 5 wt %, 10 wt % and 15 wt % in the photocatalysts were labelled as MCMN/STO-5, MCMN/STO-10 and MCMN/STO-15, respectively.

Characterization

X-ray powder diffraction (XRD) patterns were recorded by a Rigaku Ultima IV X-ray diffractometer. Transmission electron microscope (TEM) and high-resolution TEM (HRTEM) images were obtained from a FEI Glacios Cryo-TEM microscope. Scanning electron microscopy (SEM) images were obtained from a FEI Quanta 200 microscope. Thermogravimetric analysis (TGA) was performed on a Shimadzu DTG-60 thermal analyser in an Ar flow. The contents of Mn and Co elements were detected by using an inductively coupled plasma atomic emission spectrometry (ICP-AES: Thermo Fisher IRIS Intrepid II XSP). Surface structure was detected by an Thermo VG Scientific

ESCALAB 250 X-ray photoelectron spectrometer. UV-visible diffuse reflectance spectra (UV-vis DRS) were obtained from a Shimadzu UV-3600UV-visible spectrophotometer. Photoluminescence (PL) spectra were detected by a fluorescence spectrophotometer with an excitation wavelength of 389 nm. PL decay plots were obtained from an Edinburgh Instruments F980 fluorescence lifetime spectrophotometer. Electron Paramagnetic Resonance (EPR) spectra were recorded by of a Bruker EPR A300-10/12 spectrometer in a DMPO solution with methanol dispersion for DMPO$-^.O^{2-}$ and aqueous dispersion for DMPO$-^.OH$, respectively.

Photocatalytic overall water splitting

Photocatalytic overall water splitting tests were carried out in a closed photocatalytic reaction system (Labsolar-6A, Beijing Perfectlight). A 300 W Xe-lamp (PLS-SXE300D, Beijing Perfectlight) was used as the light source. In a typical experiment, 20 mg of photocatalyst was suspended in 100 mL pure water in a Pyrex glass reaction cell at 15°C by a flow of cooling water. Before irradiation, the photocatalytic reaction system was evacuated for 30 min to remove air completely. The evolved H_2 and O_2 were detected by an online gas chromatograph (GC7900, TCD with Ar as the carrier gas).

The stability of photocatalyst was tested. After 10 hours of reaction, the generated H_2 and O_2 were evacuated completely, followed by another 10 hours of reaction. According to the H_2 generation under monochromatic light illumination, the apparent quantum efficiency (AQE) was calculated by Eq. 1,[1, 2]

$$AQE = \frac{2 \times N_{H_2}(S^{-1} \cdot cm^{-2})}{P_\lambda(mW \cdot cm^{-2}) \div E_\lambda(mW \cdot s^{-1})} \times 100 \%$$

(1)

where N_{H_2} is the molecules number of the produced H_2, λ is the wavelength of the irradiated monochromatic light, E_λ and P_λ is the average photon energy and the light intensity of per unit area at corresponding λ, respectively.

Photoelectrochemical measurements

A mixed solution of 10 μL 5 wt% Nafion solution, 5.0 mg of photocatalyst and 1.0 ml ethanol was sonicated to a homogeneous dispersion. 100 μL mixed solution was droped on a FTO glass substrate (2×1 cm^2), after dried, the working electrode was obtained.

Photoelectrochemical measurements were carried out by an electrochemical workstation (CHI 650E) with a three electrode system. The Pt foil electrode and Ag/AgCl (saturated KCl) electrode were used as a counter electrode and a reference electrode, respectively. A Na_2SO_4 solution (0.5 M) was used as electrolyte for all the tests except for the electrocatalytic oxygen evolution reaction (OER). A 300 W Xe-lamp with a 400 nm cut-off filter was used as the light source. The transient photocurrent curves were recorded at bias 0.3 V. The electrochemical impedance spectra (EIS) were recorded at amplitude of 5 mV and frequency of $0.01\text{-}10^5$ Hz. The Mott-Schottky (MS) plots were recorded at amplitude of 5 mV and frequency of 1000 Hz. The flat band potentials (V_{fb}) were estimated based on the MS plots by means of Eq. 2.[3]

$$\frac{1}{C^2} = [\frac{2}{e_0 \varepsilon \cdot \varepsilon_0 N_d A^2}][E - E_{fb} - \frac{KT}{e}]$$

(2)

Where C is the space charge layer capacitance, N_d stands for the electron donor density, e_0 stands for the electron charge, E denotes the applied potential, ε and ε_0

represent the material's permittivity and permittivity of vacuum, respectively. V_{fb} is calculated by extrapolating the fitted line at $C^{-2} = 0$. The polarization curves of electrocatalytic hydrogen evolution reaction (HER) were recorded at a scan rate of 5 mV s^{-1}. The polarization curves of electrocatalytic OER were recorded at a scan rate of 5 mV s^{-1} in a KOH solution (1.0 M). To obtain potential to reversible hydrogen electrode (RHE), Eq. 3 was employed.

$$E_{RHE} = E_{AgCl} + 0.059pH + E_{AgCl}^0 (E_{AgCl}^0 = 0.197V) \tag{3}$$

Part II: Supplementary Results
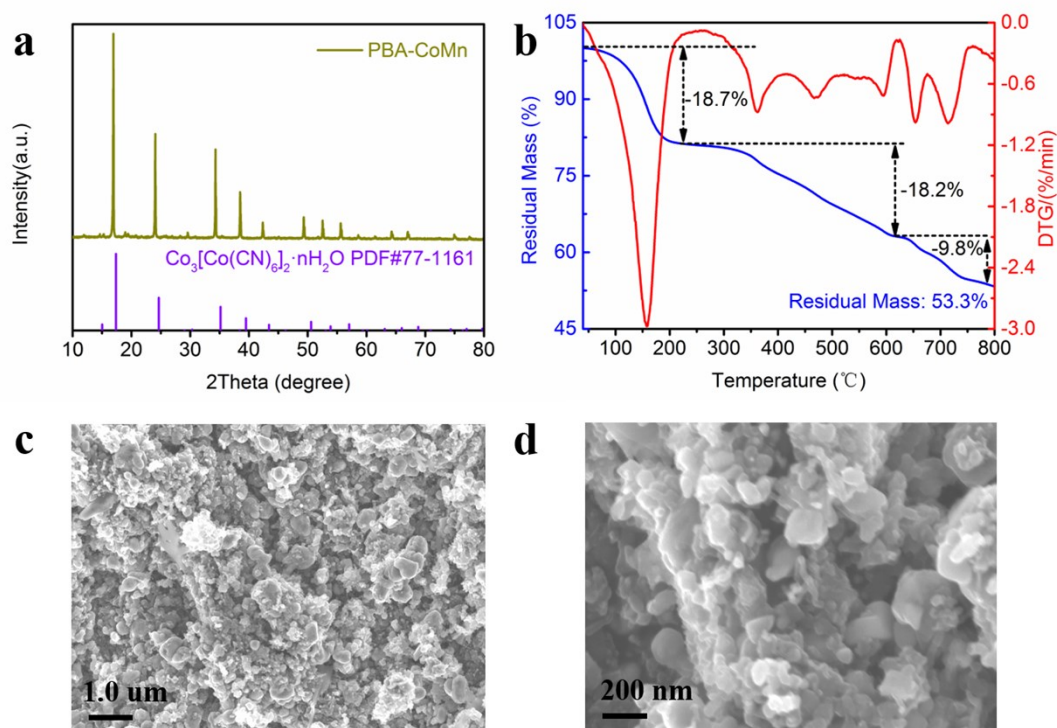
Figure S1. The XRD pattern (a) and TG analysis (b) of PBA-CoMn. The SEM images (c, d) of MCMN.

XRD pattern (**Figure S1a**) confirms that the peaks of PBA-CoMn closely match cubic $Co_3[Co(CN)_6]_2 \cdot nH_2O$ (JCPDS 77-1161). The slight shift to lower angles for the PBA-CoMn, relative to $Co_3[Co(CN)_6]_2 \cdot nH_2O$, owing to the substitution of Co^{2+} by Mn^{2+} having a larger radius. Determined by ICP-AES, the exact contents of Co and Mn in the MCMN are 22.12 wt % and 30.20 wt %, that is, the molar mass ratio of Co/Mn is close to 4:6, respectively. In addition, the weight percentage of N-doped graphitic carbon is 47.68 wt %. And the N-doped graphite carbon comes from the pyrolysis and graphitization of cyanogroup.
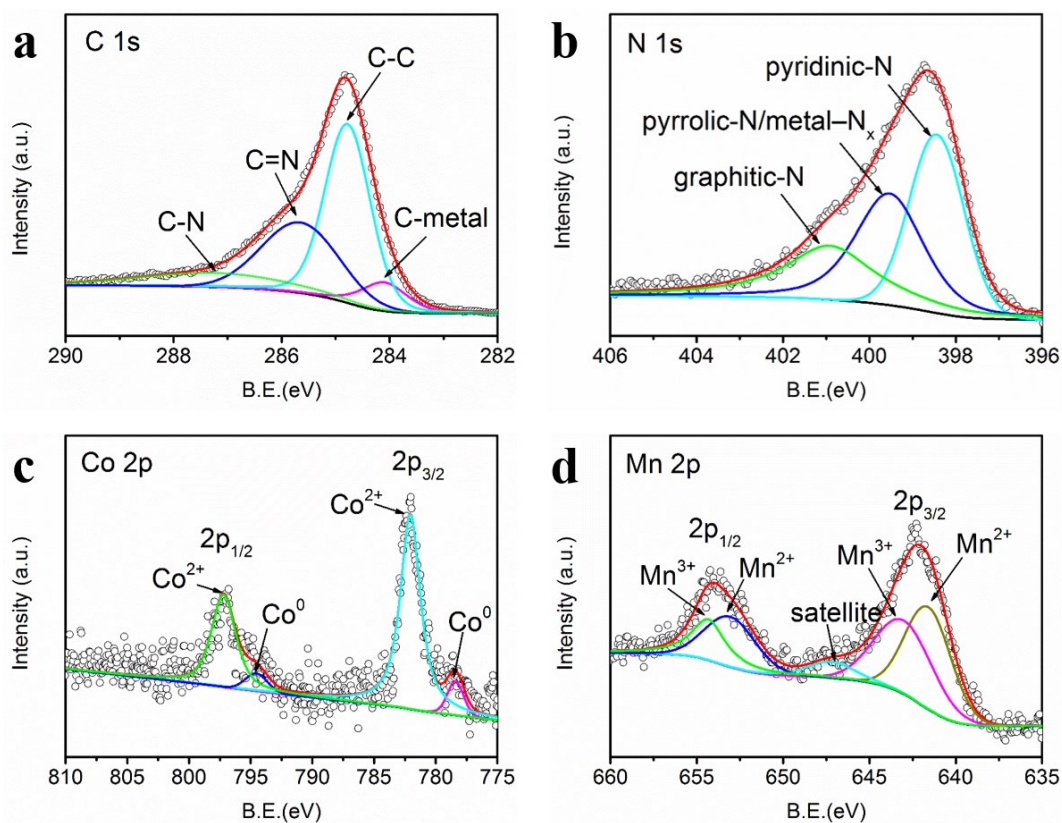
Figure S2. The high-resolution XPS spectra of MCMN: C 1s (a), N 1s (b), Co 2p (c) and Mn 2p (d).

Figure S2 shows the high-resolution C, N, Co and Mn spectra of MCMN. The high-resolution C 1s spectra can be divided into four peaks, three peaks are the C–C band (284.78 eV), C=N bond (285.65 eV) and C–N (287.24 eV) of N-doped graphitic carbon shell, respectively.[4] The peak of 284.11 is indexed to the C–metal band of Mn_2Co_2C.[5] The high resolution N 1s spectra show three peaks of doped N elements at 398.44 eV (pyridinic–N), 399.53 eV (pyrrolic–N/Co–N_x) and 404.91 eV (graphitic-N).[6] The binding energies of 782.06 and 797.12 eV in the Co 2p spectra are assigned to Co^{2+},[7] ascribed to the surface oxidation of Mn_2Co_2C. The binding energy of 778.40 eV and 794.54 are assigned to Co^0 in an alloy.[4, 5] The high-resolution Mn 2p spectra can be divided into

five peaks, two peaks at binding energies of 641.59 and 653.07 eV are associated with

Mn^{2+}, and the other two peaks of 643.03 and 654.32 eV are associated with Mn^{3+},

suggesting the presence of $Mn_2N_{0.86}$,[5] while the one of 647.20 eV are the satellite
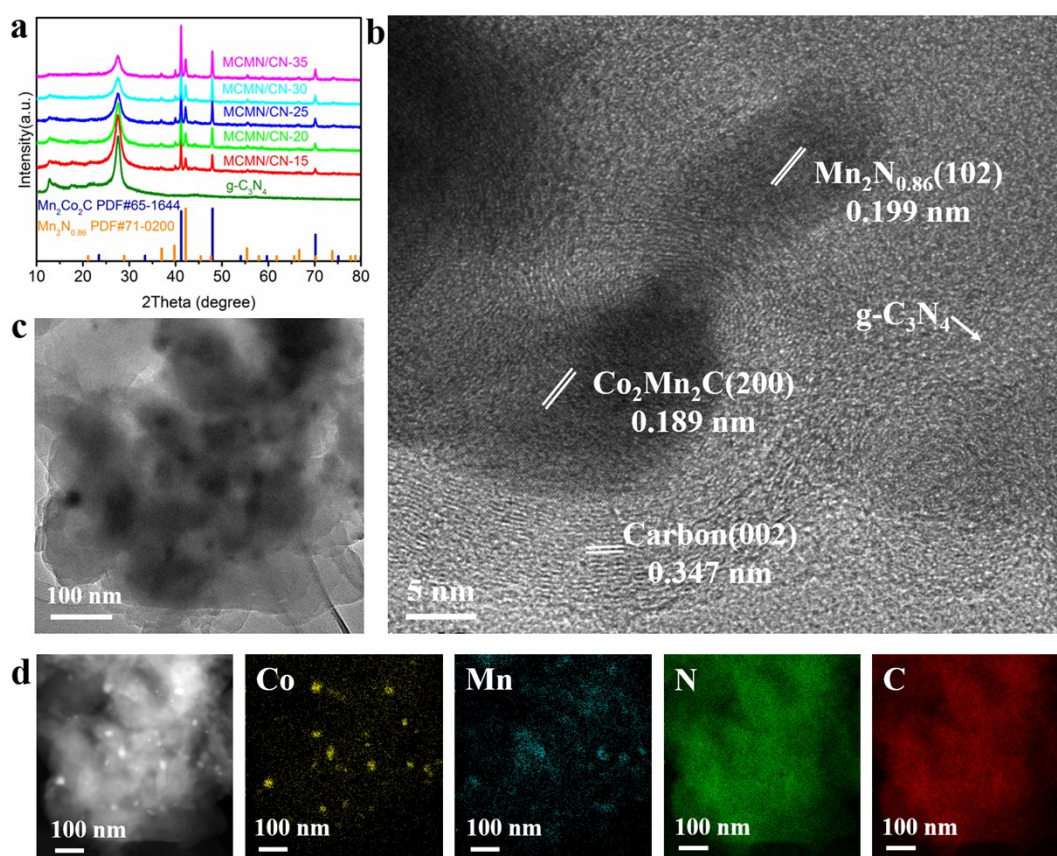
peak.

Figure S3. The XRD patterns (a) of MCMN/CN photocatalysts. The HTEM (b), TEM (c),

STEM (d) images and the corresponding elemental mappings of MCMN/CN-15.

As presented in **Figure S3a**, the XRD pattern of g-C_3N_4 exhibits two peaks at 2θ =

13.26 and 27.52° indexed to the (100) and (002) lattice planes, respectively.[8] The XRD

patterns of MCMN/CN photocatalysts match well with MCMN and g-C_3N_4. Notably,

the intensities of characteristic diffraction peaks of MCMN increase gradually with the increased content, whereas those of the g-C_3N_4 decrease, indicating that the crystal structure of g-C_3N_4 is markedly covered by the loading of MCMN on its surface.

The TEM image (**Figure S3c**) of MCMN/CN-15 reveals that MCMN hydrids are uniformly embedded on g-C_3N_4 nanosheets, further confirmed by STEM image and elemental mappings (**Figure S3d**). The uniform dispersions of Co and Mn confirm MCMN hydrids are evenly loaded on g-C_3N_4. HRTEM image (**Figure S3b**) proves that MCMN nanoparticles are welded onto g-C_3N_4 nanosheets. A core has lattice plane with d-spacing of 0.189 nm, corresponded to the (200) plane of Mn_2Co_2C. An adjacent lattice plane with a d-spacing of 0.199 nm is assigned to the (102) plane of $Mn_2N_{0.86}$. Meanwhile, Mn_2Co_2C cores are coated by N-doped graphitic carbon shells (lattice fringes of 0.347 nm). The above results confirmed that MCMN were successfully embedded on the surface of g-C_3N_4 to fabricate a high quality photocatalyst.
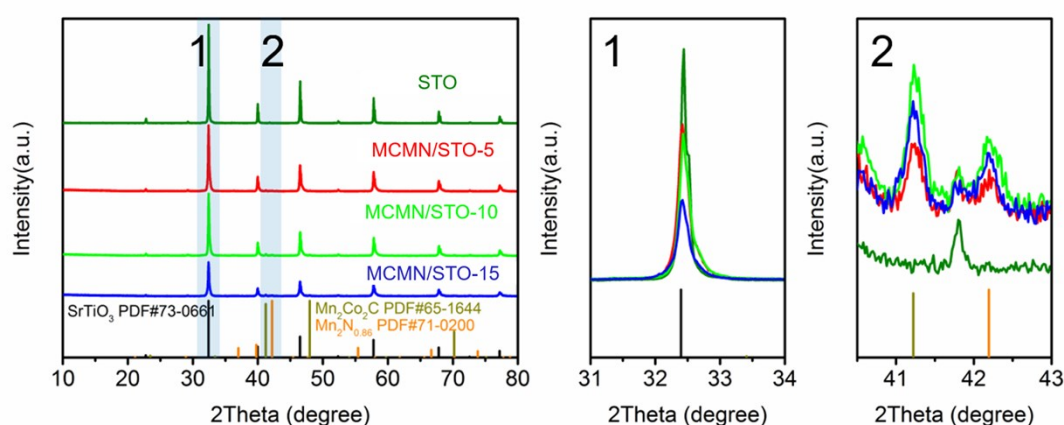

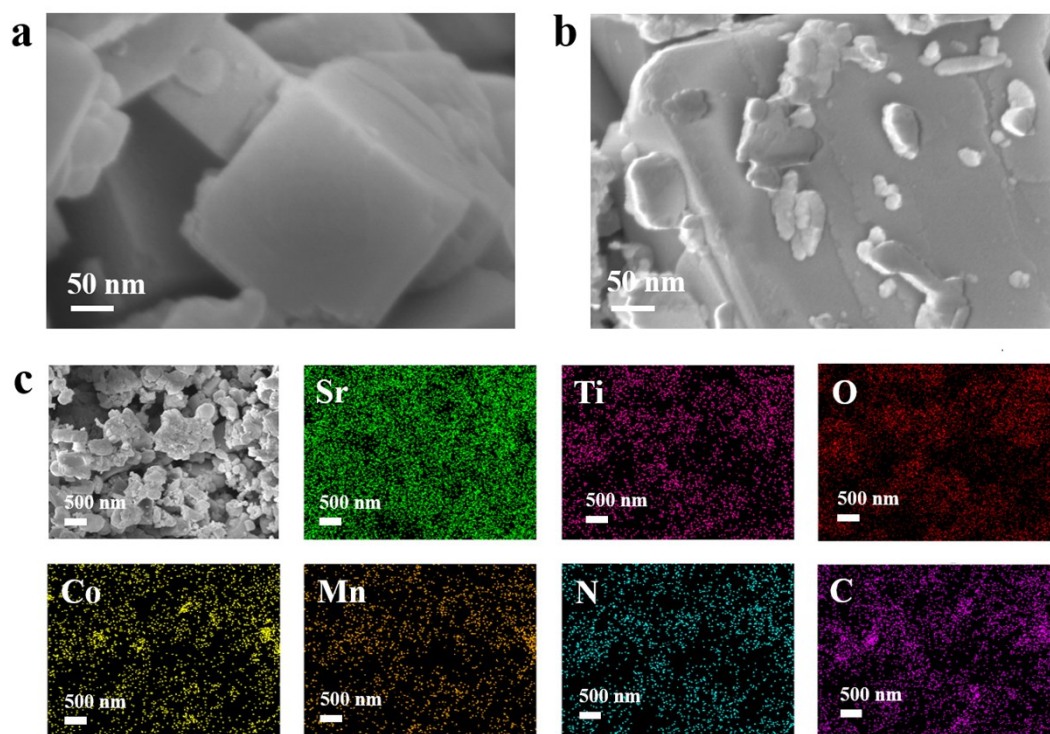**Figure S4.** The XRD patterns of $SrTiO_3$ and MCMN/STO photocatalysts.

Figure S5. The SEM image of SrTiO$_3$ (a), the SEM images of MCMN/STO-10 (b, c) and the corresponding elemental mappings of picture c.
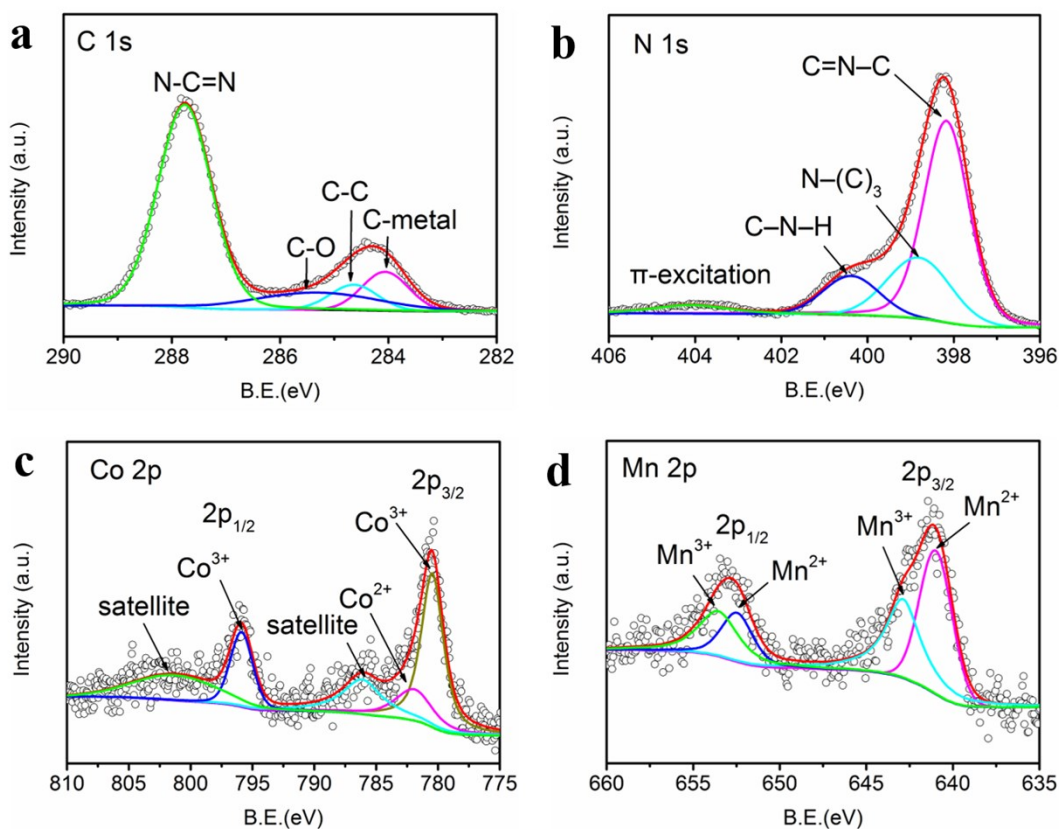
Figure S6. The high-resolution XPS spectra of recycled MCMN/CN-30: C 1s (a), N 1s (b), Co 2p (c) and Mn 2p (d).

Figure S6 shows the high-resolution C, N, Co and Mn spectra of recycled-MCMN/CN-30. The high-resolution C 1s spectra can be divided into four peaks, two peaks are C–O band (285.32 eV) and N–C=N bond (287.76 eV) of g-C$_3$N$_4$.[9, 10] The other peaks of 284.06 and 284.64 eV are indexed to the C–metal band of Mn$_2$Co$_2$C and the C–C of graphitic carbon shell, respectively.[4, 5] The high resolution N 1s spectra show four peaks of g-C$_3$N$_4$ at 398.17 eV (C=N–C), 398.81 eV [N–(C$_3$)], 400.38 eV (C–N–H) and 404.09 eV (π-excitation).[11] The binding energies of 780.45 and 795.88 eV in the Co 2p spectra are assigned to Co^{3+},[12] ascribed to the surface oxidation of Mn$_2$Co$_2$C. The binding energy of 781.92 eV is assigned to Co^{2+} of Mn$_2$Co$_2$C,[13] while the ones of 786.13

and 801.27 eV are the satellite peaks. The high-resolution Mn 2p spectra can be divided into four peaks, two peaks at binding energies of 640.99 and 652.47 eV are associated with Mn^{2+}, and the other two peaks of 642.88 and 653.54 eV are associated with Mn^{3+}.[14] In addition, the energy separation between Mn $2p_{1/2}$ and Mn $2p_{3/2}$ is 11.87 eV, demonstrating the presence of MnOOH.[14] Based on the XRD, HRTEM and XPS results, it is summarized that the recycled-MCMN/CN-30 is comprised of g-C_3N_4, $Mn_2Co_2C@C$ and MnOOH, in which the $Mn_2Co_2C@C$ and MnOOH are loading on the surfaces of g-C_3N_4 with tight and robust structures.
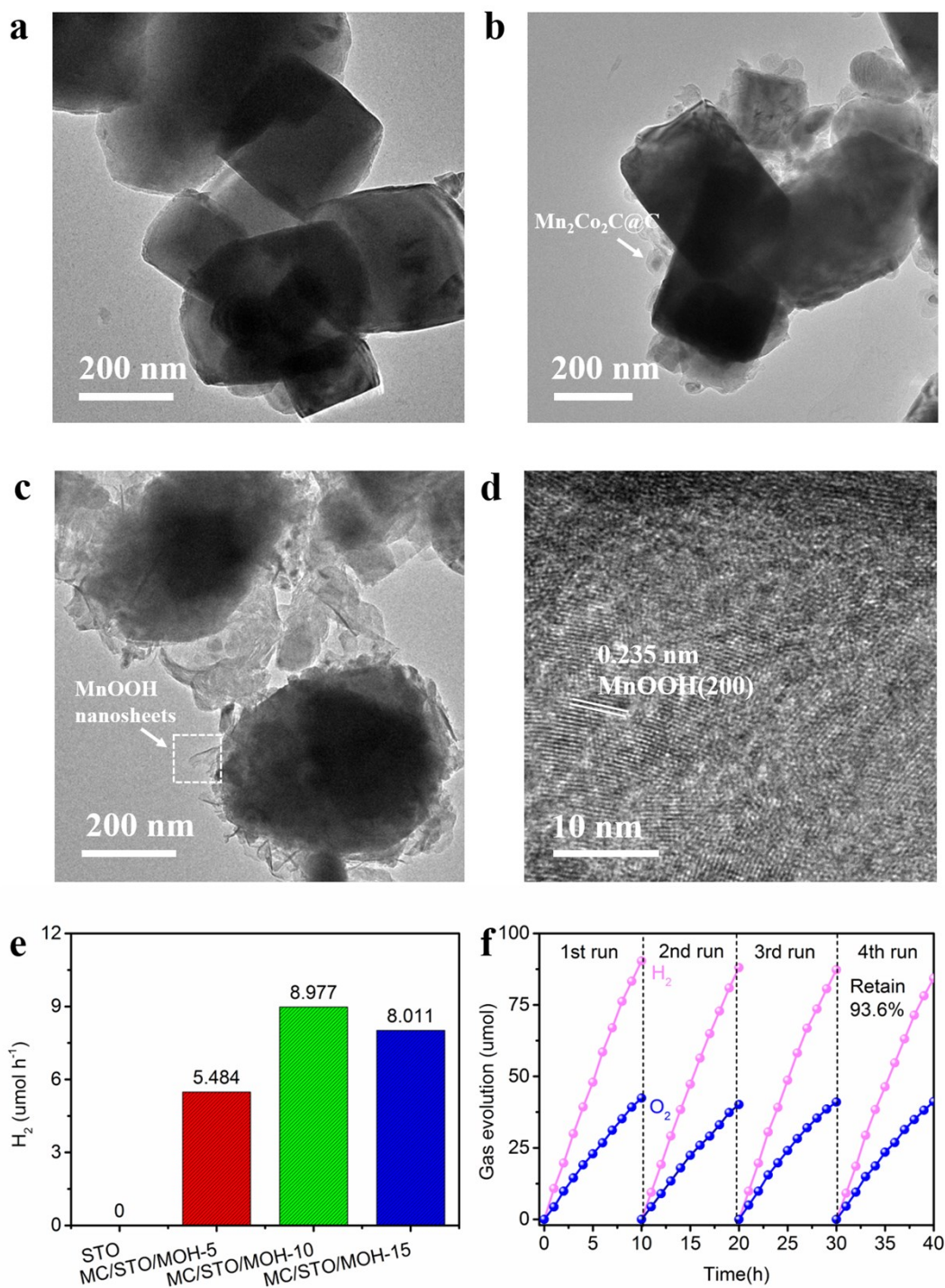
Figure S7. The TEM and HRTEM images: (a) SrTiO$_3$, (b) as-prepared MCMN/STO-10, (c) MC/STO/MOH-10, (d) selection in c. The photocatalytic performances under UV-vis light irradiation in pure water (50 mg of photocatalyst): (e) average H$_2$ evolution rates of MC/STO/MOH samples, (f) stability tests of MC/STO/MOH-10.
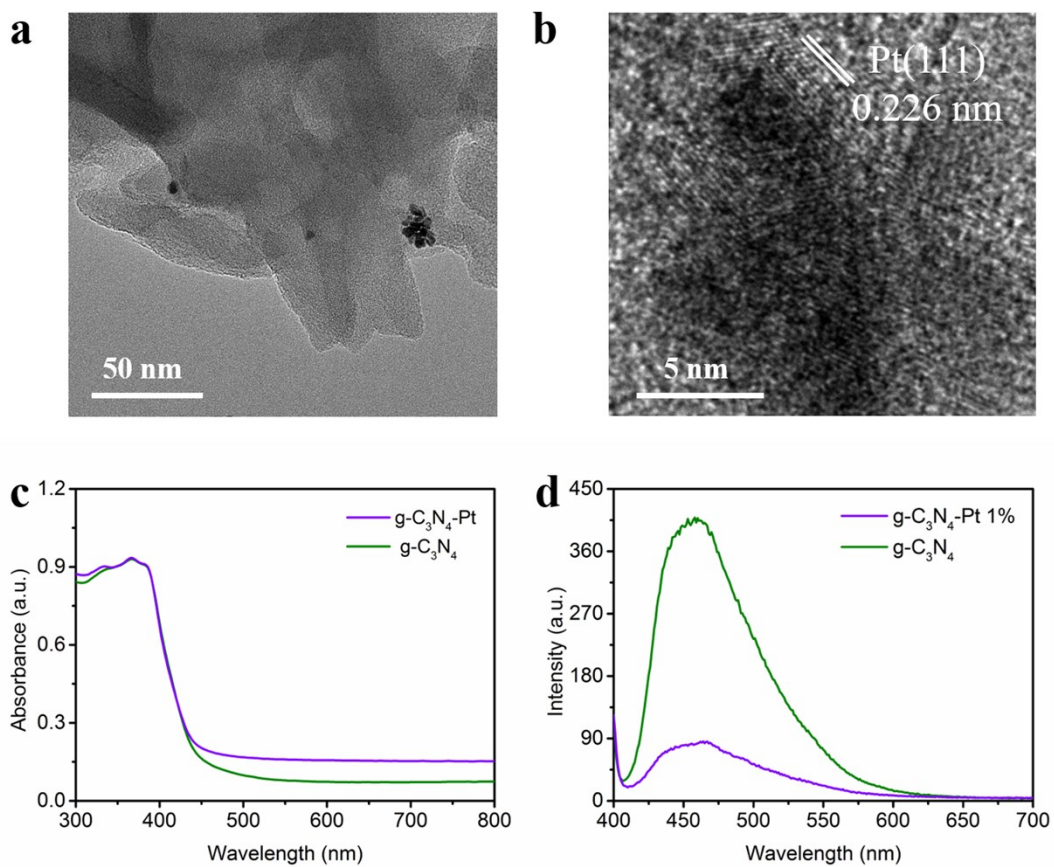
Figure S8. The TEM (a) and HRTEM (b) images of g-C$_3$N$_4$-Pt, The UV-vis diffuse reflectance spectra (c) and photoluminescence spectra (d) of g-C$_3$N$_4$ and g-C$_3$N$_4$-Pt.
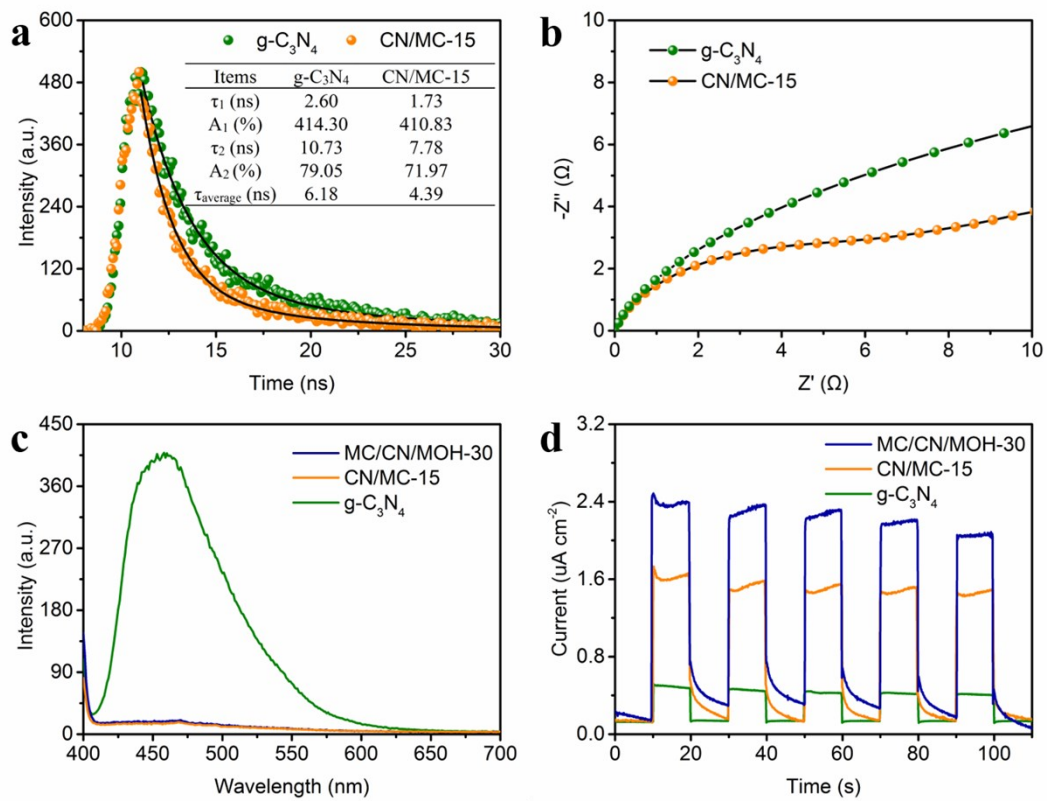
Figure S9. The transient PL spectra (a) and electrochemical impedance spectroscopy (b) of g-C_3N_4 and CN/MC-15. The PL spectra (c) and transient photocurrent response test (d) of g-C_3N_4, CN/MC-15 and MC/CN/MOH-30.
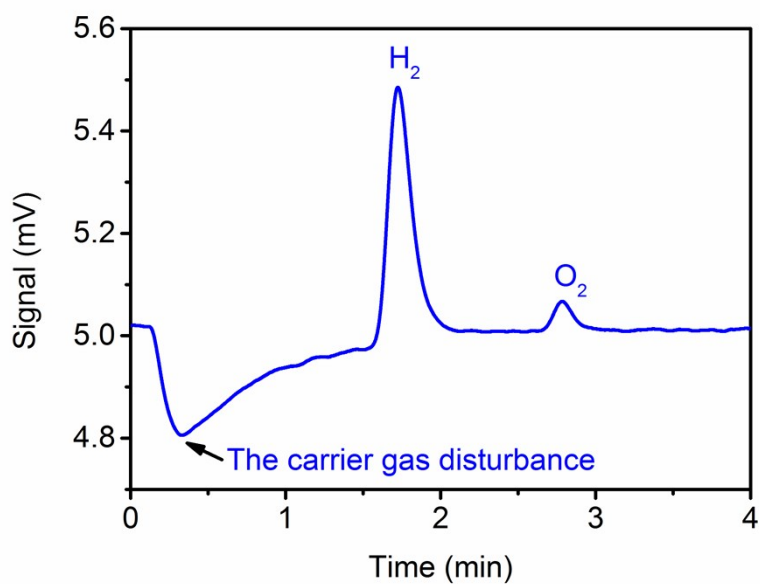
Figure S10. The actual H_2 and O_2 testing chart detected by gas chromatography over MC/CN/MOH-30 photocatalyst.

The typical GC raw data of photocatalytic overall water splitting over MC/CN/MOH-30 photocatalyst is shown in **Figure S10**, the negative peak at 0.33 min is ascribed to the carrier gas disturbance during injection. The peaks at 1.72 min and 2.78 min are assigned to H_2 and O_2, respectively. Based on the peak areas of H_2 and O_2, the amount of H_2 and O_2 can be calculated by external standard method.

Table S1. Summary of the photocatalytic H_2 evolution on g-C_3N_4 based photocatalysts for overall water splitting.

Photocatalysts	Cocatalysts	Power (Xe lamp), wavelength	Activity (μmol h^{-1} g^{-1})	AQE	Reference (year)
g-C_3N_4	Mn_2Co_2C@C/MnOOH	300W	64.15	1.45% at 420 nm	This work
g-C_3N_4	Pt/PtO$_x$/CoO$_x$	300W	61	0.3% at 405 nm	[15](2016)
g-C_3N_4	Pt/Co$_3$O$_4$	300W	610	/	[16](2016)
α-Fe$_2$O$_3$/g-C_3N_4	Pt/RuO$_2$	300W, $\lambda \geq$ 420 nm	38.2	/	[17](2017)
g-C_3N_4	Co$_1$-phosphide	300W, $\lambda \geq$ 420 nm	126.8	3.6% at 420 nm	[18](2017)
g-C_3N_4	Au	300W, $\lambda \geq$ 420 nm	150.1	/	[19](2018)
CoO/g-C_3N_4	/	LED, $\lambda \geq$ 400 nm	50.2	1.91% at 420 nm	[20](2018)
g-C_3N_4	NiO	300W, $\lambda \geq$ 420 nm	28	/	[21](2018)
g-C_3N_4	Pt/Ni(OH)$_2$	300W	425.7	1.8% at 420 nm	[22](2019)
g-C_3N_4	Pt@Ni(OH)$_2$/Pt	300W	1330	4.2% at 420 nm	[23](2019)
g-C_3N_4/Ti$_3$C$_2$	Pt	300W, $\lambda \geq$ 420 nm	627.1	8.7% at 350 nm	[24](2019)
g-C_3N_4-RGO-Fe$_2$O$_3$	Pt	300W	1090	/	[25](2019)
MnO$_2$/g-C_3N_4	Pt	300W, $\lambda \geq$ 420 nm	60.6	/	[26](2019)
Mn-g-C_3N_4	Pt	300W, AM1.5	695.1	4.0% at 420 nm	[27](2019)
P-g-C_3N_4	Pt/CoP	300W, $\lambda \geq$ 420 nm	213.6	6.8% at 400 nm	[28](2020)
CdS/g-C_3N_4	Pt/MnO$_x$	300W, $\lambda \geq$ 420 nm	924.4	1.745% at 420	[29](2020)

Part III: References

1. J. Song, H. Zhao, R. Sun, X. Li and D. Sun, *Energy Environ. Sci.*, 2017, **10**, 225-235.
2. X. Zhou, Q. Gao, S. Yang and Y. Fang, *Chinese Journal of Catalysis*, 2020, **41**, 62-71.
3. Z. Lin and X. Wang, *Angew. Chem. Int. Ed.*, 2013, **52**, 1735-1738.
4. X. Zhou, Y. Zhu, Q. Gao, S. Zhang, C. Ge, S. Yang, X. Zhong and Y. Fang, *ChemSusChem*, 2019, **12**, 4996-5006.
5. C. Deng, K.-H. Wu, J. Scott, S. Zhu, R. Amal and D.-W. Wang, *J. Mater. Chem. A*, 2019, **7**, 20649-20657.
6. S. Chen, X. Zhou, J. Liao, S. Yang, X. Zhou, Q. Gao, S. Zhang, Y. Fang, X. Zhong and S. Zhang, *J. Mater. Chem. A*, 2020, **8**, 3481-3490.
7. D. Zhu, Y. Huang, J.-j. Cao, S. C. Lee, M. Chen and Z. Shen, *Appl. Catal. B-Environ.*, 2019, **258**, 117981.
8. G. Zhang, Z.-A. Lan and X. Wang, *Chem. Sci.*, 2017, **8**, 5261-5274.
9. L. Luo, K. Li, A. Zhang, H. Shi, G. Zhang, J. Ma, W. Zhang, J. Tang, C. Song and X. Guo, *J. Mater. Chem. A*, 2019, **7**, 17815-17822.
10. P. Xia, M. Antonietti, B. Zhu, T. Heil, J. Yu and S. Cao, *Adv. Funct. Mater.*, 2019, **29**, 1900093.
11. Z. Pan, G. Zhang and X. Wang, *Angew. Chem.*, 2019, **131**, 7176-7180.
12. L. Zhuang, L. Ge, Y. Yang, M. Li, Y. Jia, X. Yao and Z. Zhu, *Adv. Mater.*, 2017, **29**, 1606793.
13. X. Ma, K. Li, X. Zhang, B. Wei, H. Yang, L. Liu, M. Zhang, X. Zhang and Y. Chen, *J. Mater. Chem. A*, 2019, **7**, 14904-14915.
14. Y. Wang, T. Hu, Q. Liu and L. Zhang, *Chem. Commun.*, 2018, **54**, 4005-4008.
15. G. Zhang, Z.-A. Lan, L. Lin, S. Lin and X. Wang, *Chem. Sci.*, 2016, **7**, 3062-3066.
16. D. Zheng, X.-N. Cao and X. Wang, *Angew. Chem. Int. Ed.*, 2016, **55**, 11512-11516.
17. X. She, J. Wu, H. Xu, J. Zhong, Y. Wang, Y. Song, K. Nie, Y. Liu, Y. Yang, M.-T. F. Rodrigues, R. Vajtai, J. Lou, D. Du, H. Li and P. M. Ajayan, *Adv. Energy Mater.*, 2017, **7**, 1700025.
18. W. Liu, L. Cao, W. Cheng, Y. Cao, X. Liu, W. Zhang, X. Mou, L. Jin, X. Zheng, W. Che, Q. Liu, T. Yao and S. Wei, *Angew. Chem. Int. Ed.*, 2017, **56**, 9312-9317.
19. J. Bai, B. Lu, Q. Han, Q. Li and L. Qu, *ACS Appl. Mater. Interfaces*, 2018, **10**, 38066-38072.
20. F. Guo, W. Shi, C. Zhu, H. Li and Z. Kang, *Appl. Catal. B-Environ.*, 2018, **226**, 412-420.
21. Y. Fu, C. a. Liu, C. Zhu, H. Wang, Y. Dou, W. Shi, M. Shao, H. Huang, Y. Liu and Z. Kang, *Inorg. Chem. Front.*, 2018, **5**, 1646-1652.
22. S. Sun, Y.-C. Zhang, G. Shen, Y. Wang, X. Liu, Z. Duan, L. Pan, X. Zhang and J.-J. Zou, *Appl. Catal. B-Environ.*, 2019, **243**, 253-261.
23. S. Sun, Y. Feng, L. Pan, X. Zhang and J.-J. Zou, *Appl. Catal. B-Environ.*, 2019, **259**, 118028.
24. Z. Ai, Y. Shao, B. Chang, L. Zhang, J. Shen, Y. Wu, B. Huang and X. Hao, *Appl. Catal. B-Environ.*, 2019, **259**, 118077.
25. Z. Pan, G. Zhang and X. Wang, *Angew. Chem. Int. Ed.*, 2019, **58**, 7102-7106.
26. Z. Mo, H. Xu, Z. Chen, X. She, Y. Song, J. Lian, X. Zhu, P. Yan, Y. Lei, S. Yuan and H. Li, *Appl. Catal. B-Environ.*, 2019, **241**, 452-460.
27. S. Sun, G. Shen, J. Jiang, W. Mi, X. Liu, L. Pan, X. Zhang and J.-J. Zou, *Adv. Energy Mater.*, 2019, **9**, 1901505.
28. Z. Qin, Z. Huang, M. Wang, D. Liu, Y. Chen and L. Guo, *Appl. Catal. B-Environ.*, 2020, **261**, 118211.
29. X. Zhou, Y. Fang, X. Cai, S. Zhang, S. Yang, H. Wang, X. Zhong and Y. Fang, *ACS Appl. Mater.*

Interfaces, 2020, **12**, 20579-20588.